Design of a Micro Air Vehicle through Bio-mimicry of Bumblebees

Authors: Michael Thompson* ,Akshay Batra and Deyzi Ixtabalan †John Burnett ‡
Diana Tran §
Advisors: Dr. Armando Rodriguez, Dr. Marcus Herrmann¶,and Dr. Bruce Steele ‖
Arizona State University, Tempe, AZ, 85287, United States

This research focuses on aerodynamic characteristics of a recently developed Micro Air Vehicle (MAV)-like bumblebee. The MAV prototype has a flexible membrane with an aspect ratio of 4.18 and a chord of 8 cm. The aspect ratio of a typical queen bumblebee is 5.78.[1] One wing area is 90.38 cm^2 measured from the SolidWorks model and an inner area-fuselage of 6.78 cm^2. The planform area, S was calculated as 187.56 cm^2. The Reynolds number (Re) of approximately 62,000 was used for the wind tunnel testing as MAVs typically fly at low Re. The bumblebees dynamic wing behavior is able to articulate in one degree of freedom-flapping back and forth. The wing span, b of the prototype is 28 cm. The current MAV model was designed through SolidWorks and manufactured using 3D printing to build this rapid prototype. The rapid prototype would replicate a real bumblebee mimicking its articulation and aerodynamic attributes. The current MAV prototype has a 12 volt six winding brushless motor with a maximum capacity of 8,750 rpm to provide hovering equilibrium which presented a constant challenge in the previous prototypes. Numerical simulations of the air flow that surrounds the bumblebee wing is presented using an incompressible Navier-Stokes solver with ANSYS-FLUENT. A computational grid has 64,297 nodes and 300,000 elements. The maximum computational lift coefficient is approximately 0.5045 at 25 degrees angle of attack (AOA). Experimentally, from wind tunnel testing the lift coefficient is 0.5894. A stall angle was observed at 16 degrees angle of attack. A minimum drag coefficient was calculated to be -0.2389 at -7 degrees AOA. The experimental data collection was intended to find the aerodynamic derivatives that will be helpful, in the future, to model the micro air vehicles flight control system with MATLAB and Simulink.

AOA	Angle of Attack
D	Drag
L	Lift
P	Pressure, Pa
V	Velocity, m/s
c_l	Lift Coefficient
c_d	Drag Coefficient
x, y, z	Cartesian body axes, m
α	Angle of attack, deg
ρ	Density, kg/m^3

*Group Leader, working towards PhD in Micro Air Vehicle technology, AIAA member.
†Graduate students, currently working on CFD for Micro Air Vehicles, AIAA members.
‡Project Engineer, currently working at Honeywell, AIAA members.
§Undergraduate Mechanical Engineer, currently working on CFD for MAVs, AIAA member.
¶Professors, IEEE and AIAA members.
‖Laboratory Manager, AIAA member.

I. Introduction

Micro air vehicles have developed through the years, in different dimensional configurations; however, no standard configurations have been established by the aerospace community.[4] Fixed wing aircraft and helicopter blade elements have well established algorithms to predict design efficiency, although flapping wing micro air vehicle designs are typically being based off nature and bio-mimicry.[1,2] Micro air vehicles are rising as the focus of study for multifunctional purposes. The ASU bumblebee is 6 cm long in fuselage direction, 3.1 cm wide in the chord wise direction, 11.8 cm tall and has a wing span of 28 cm. This work involves developing vehicles with low aspect ratio wings that operate at low Reynolds numbers.

The MAV prototype was modeled after a bumblebees anatomy and articulation behavior.[8,9,10] The current MAV design was made through many different wing design changes. The current wings were modeled similar to the wings of a bee, which are more aerodynamic.

Micro air vehicles are rising as the focus of study for multifunctional purposes. The prototypes are being designed to accommodate such purposes as search and rescue and reconnaissance.

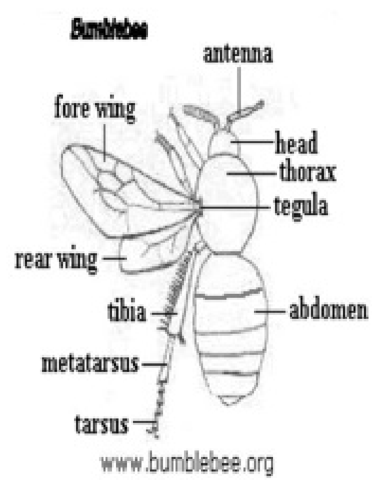

Figure 1: Anatomy of a real bumblbee.

II. ASU MAV Design

Due to the sizing of the MAV capabilities special attention is required for a range of power and weight; these requirements must be appraised. Much attention is needed in the computational fluid dynamics arena for the MAV wings. This area is one of the utmost concerns because the aerodynamics is least understood in MAVs.[4] Unsteady aerodynamics play a critical role for MAV flight stability and control concerns.[12,13,14] Typically, MAVs are small in size and weigh below 100 grams.[6,7] The ASU bumblebee MAV is approx. 98.6 grams and carbon fiber spars with a Youngs Modulus of 150 GPa as can be seen in the figure below.

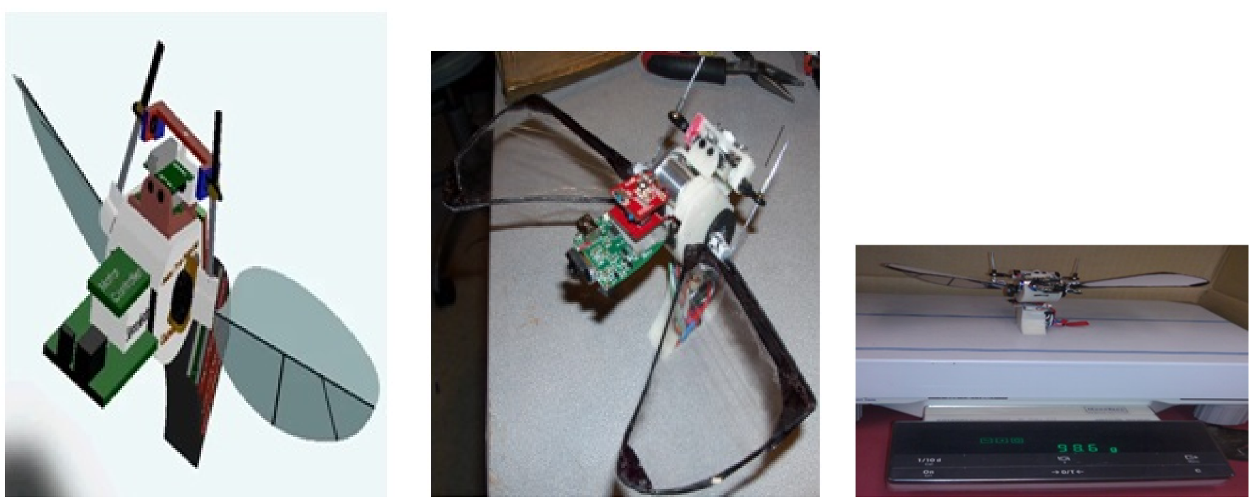

(a) The CAE SolidWorks model of the recently designed Bumblebee MAV.

(b) The actual model of the Bumblebee MAV.

(c) Weighs approx. 98.6 grams with PID controller, camera, brushless motor, Li-PO battery and wings.

Figure 2: ASU Bumblebee MAV, a flexible wing micro air vehicle geometrically modeled, designed, fabricated, and tested at Arizona State University.

The design for our bumblebee MAV was made to replicate a bumblebee for its aerodynamic attributes. The bumblebee MAV prototype was designed using ABS plastic via rapid prototyping-3D printing. The vehicle uses a brushless motor to increase the lifting capabilities in comparison to a brush-equipped motor. The current MAV contains 6 Li-Po batteries. The yield strength of ABS plastic (from 3D printer) is not suitable for the arm joint of the vehicle due to the compressive stress placed on the joint that causes buckling. Surpassing the yield strength for the arm joint would introduce deformation and fatigue leading up to possible cracks. Tin was used for the arm joint to withstand the compressive stress.

The manufacturing process of the Bumblebee exoskeleton and wing assemblies are designed using printing technology and carbon fiber. Part printing technology is used for building all static structural components as well as some dynamic components such as the wing-root, feathering controls and cycloid structure. Issues arising from the parts printer typically involve extruder, nozzle calibration and platform/part adhesion. A procedure for calibrating the extruder is well documented; however, it is not always the most effective method of calibration. The MakerBot Replicator 2 was used and with the software package called Makerware that sets up the way the part will be printed. Temperature, part density, number of shells, and print speed govern the quality and weight of the parts being printed. Adhesion to the platform can be an issue if a bonding pad is not integrated into the part from the SolidWorks model.

The current MAV design is incorporating insect flight structures for functional wing morphology and evolution purposes to effectively enhance flight performance. In addition to the wing dynamics, the current prototype has no sharp edges and provides a more elegant profile.

Table 1: ASU Bumblebee MAV Parameters

Parameter	Nominal Value
Wing Span	28 cm
Aspect Ratio	4.18
Airfoil stall angle	16 degrees
Max Speed	12.88 m/s
Chord length	0.08 m
Area of wing	0.009038 m^2

By placing other screws around the outside, we were able to hold the carbon fiber in place. Now, we have purchased carbon fiber strands that we are able to wrap around the wing-manufacturing template. By applying resin, we can stiffen the carbon fiber into the desired shape. By changing our method of producing wings, the entire process has shortened to around an hour. We also purchased 3/32 Balsa Wood to place at the areas which receive higher induced stress concentration. These supports help the wing maintain its shape and reduce the chance of cracking by giving the wing a higher tensile strength.

III. Wind tunnel Results

The wind tunnel was used to obtain the aerodynamic lift and drag forces. The angle of attack for the wing was varied between -10 degrees to 25 degrees. The wind speed was 12.88 m/s. The wind tunnel sucks in air from a draft fan and pumps in air at high speed (which can be regulated).

The wind tunnel has a 30 cm by 20 cm test section with a testing speed up to 20 m/s. The wind tunnel data acts as an anchor to that which we may compare our CFD simulations.

The equations that govern the range of the MAV lift and drag forces Eq. (1), and Eq. (2) may be written as:

$$D = \frac{1}{2}\rho v^2 A C_D \tag{1}$$

$$L = \frac{1}{2}\rho v^2 A C_L \tag{2}$$

The C_D, drag coefficient and C_L, lift coefficient, are often assumed constant for simple calculations but a more realistic approach defines them in terms of the angle of attack (angle between the wing and the body of its velocity).

The maximum lift and drag coefficients obtained are given below by Eq. (3), and Eq. (4) may be written as:

(a) The flow direction of the air in the windtunnel.

(b) The fan inside the wind tunnel.

(c) An overview of the windtunnel.

Figure 3: The ASU Wind Tunnel.

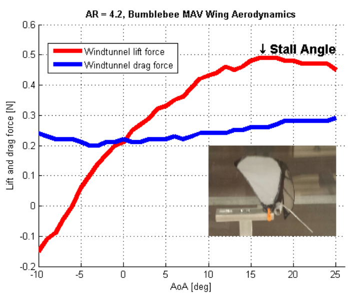

(a) Aerodynamic Forces.

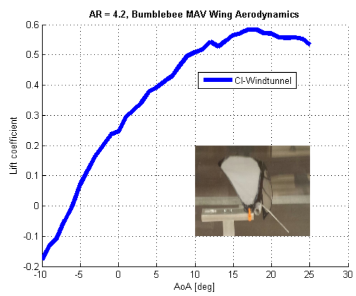

(b) Lift Coefficient vs AOA.

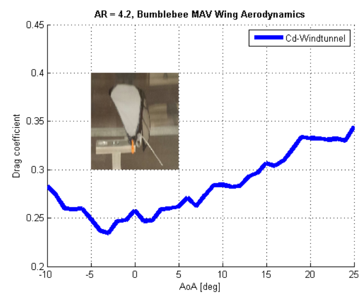

(c) Drag Coefficient vs AOA.

Figure 4: Experimental aerodynamic characteristics of the Bumblebee MAV wing from LabView.

$$C_D \cong 0.24 \tag{3}$$

$$C_L \cong 0.5902 \tag{4}$$

The aerodynamic characteristics of the Bumblebee MAV can be seen from the figures above. These characteristics examine the lift and drag as can be seen. The lift and drag coefficients are determined by the lift and drag forces.

The optimum way to approach the flight portion of the MAV should be to aim for minimum drag in the initial part of the flight and adjust for maximum lift during the flight by changing the body angle of attack.

A. Aerodynamic Efficiency

Lift divided by drag is the L/D ratio. Since lift and drag are both aerodynamic forces, L/D ratio can be thought of as an aerodynamic efficiency. The figure above shows the aerodynamic efficiency. It can be seen from the figure below that experimentally, the maximum L/D is achieved at 13 AOA and it is calculated to be approximately 1.94. The wind speed was constant at 12.88 m/s. Poor efficiency results when the MAV is flying at an angle of attack lower than 0.

B. Lift and Drag

From the figure below, the lift results show a linear increase with the AOA until the stall angle is approached. The Bumblebee MAV stall angle was seen at 16 degrees AOA where the C_L= 0.5902.

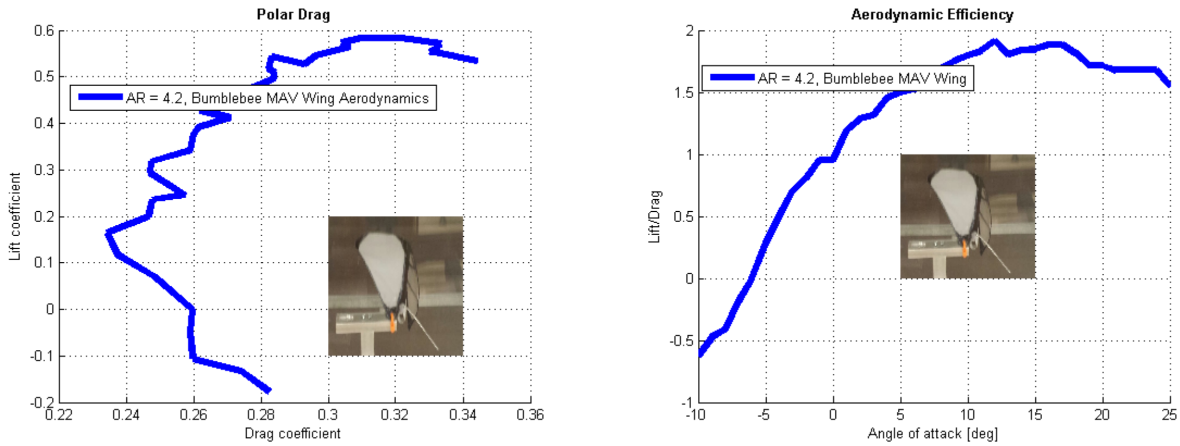

(a) Polar Drag vs AOA.

(b) Aerodynamic Efficiency.

Figure 5: Aerodynamic Characteristics of the Bumblebee MAV.

The wind tunnel air velocity blowing from left to right over the wing was low at approximately 12.88 m/s. The wings on the MAV can flap at maximum frequency of 130 Hz from experimental data taken from a tachometer.

Due to the small velocity of the air, the lift coefficient does not change much. Since the aspect ratio of our bumblebee is similar to that of a queen bee, the bumblebee MAV may have a high AOA before it stalls out. For this to occur low pressure happens at the top surface of the wing and high pressure occurs at the bottom surface of the wing. Due to this pressure differential the Bumblebee MAV wing is able to generate lift as can be seen from the experimental data collected.

The stall characteristics for insect wings are abrupt and occur at maximum lift.[9] The lift coefficient declines after this segment partially from its maximum value. The leading-edge separation bubbles may increase the camber of the wing and stop stalling.[9] The lift forces on the body in which act perpendicular to the drag may be of significance for flapping wing MAVs in regards to reducing the net lift of the beating wings.[8] In order to inhibit this stall effect the wings may be flapping. From flexible wings wind tunnel data at a stall angle of 20° with an aspect ratio of 2 was reported.[1] The stall angle increases by decreasing the aspect ratio.[1] For insect wings, an abrupt stall angle does not occur.[8,9] This is shown in Figure 5 where after an attainment of maximum lift, that is typical of airfoils of an abrupt stall angle, is not seen. Furthermore, for higher aspect ratio wings it is known to have a higher lift coefficient. In order to fly with minimum drag the bumblebee MAV should have an AOA of -5° that correspond to $C_L = 0.1$ according to the experimental wind tunnel data collected. By increasing the aspect ratio we obtain a higher lift coefficient.

IV. CFD Verification-Benchmark test for NACA 0012 airfoil

A CFD verification for the NACA 0012 airfoil is included in this case study. In the Evaluation of the turbulence models for the simulation of the flow over a National Advisory Committee for Aeronautics (NACA) 0012 airfoil work was conducted on an analysis of the two dimensional subsonic flow at various angles of attack.[15] The flow was obtained by solving the steady-state governing equations of continuity and momentum conservation combined with one of three models Spalart-Allmaras, Realizable k-ϵ, and k-ω shear stress transport (SST).[15] The aim was to validate the three models through the comparison of the predictions and the free field experimental measurements from the NACA 0012 airfoil. The work was to show the behavior of the airfoil at these conditions and to establish a verified solution method. Elen's paper worked to verify the FLUENT solver and the NACA 0012 airfoil data collection.[15]

Three simulations were conducted by Eleni[15] showing steady-state lift data for a NACA 0012 airfoil. Eleni obtained lift for various angles of attack using three FLUENT turbulent models. Then, he compared his CFD simulations with wind tunnel data and the paper showed that the most appropriate turbulent model to compare to experimental data on the NACA 0012 airfoil was the k-ω SST 2-equation model. Furthermore,

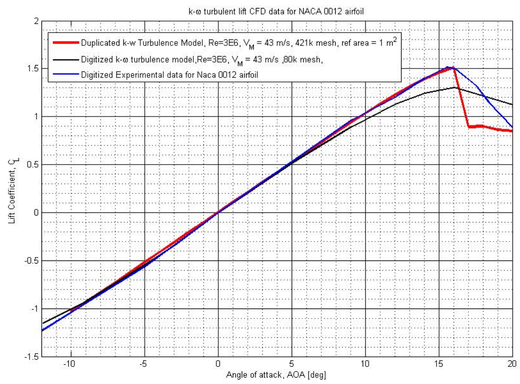

(a) Coefficient of lift data comparison between experimental data from Abbott et al and and Eleni $k-\omega$ turbulent model against the duplicated $k-\omega$ turbulent model for the NACA 0012 airfoil.

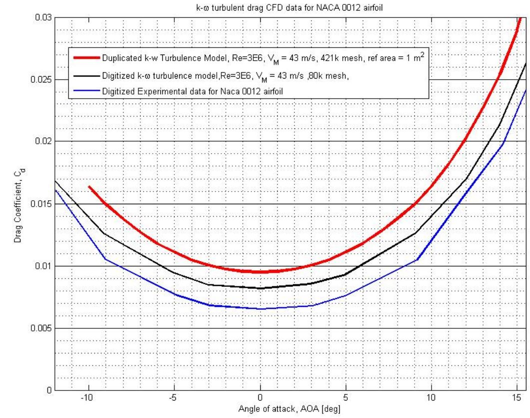

(b) Coefficient of drag data comparison between experimental data from Abbott et al and and Eleni $k-\omega$ turbulent model against the duplicated $k-\omega$ turbulent model for the NACA 0012 airfoil.

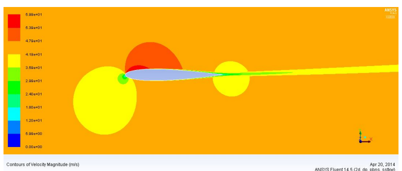

(c) Contours of velocity at 3° angle of attack with the $k-\omega$ turbulence model.

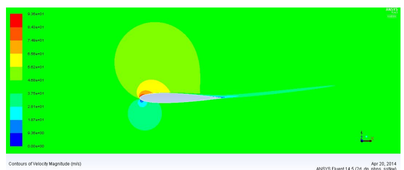

(d) Contours of velocity at 9° angle of attack with the $k-\omega$ turbulence model

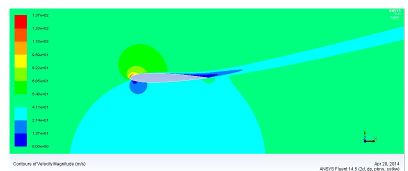

(e) Contours of velocity at 16° angle of attack with the $k-\omega$ turbulence model.

Figure 6: Comparing the contour velocity data obtained from the $k-\omega$ turbulent CFD simulation for the NACA 0012 airfoil.

in this paper we verified that the k-ω SST 2-equation model does represent the experimental data.

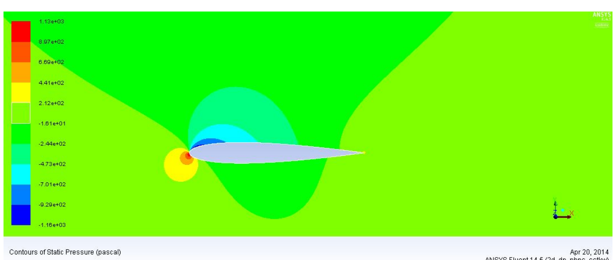

(a) Contours of static pressure at 3° angle of attack with the $k-\omega$ turbulence model.

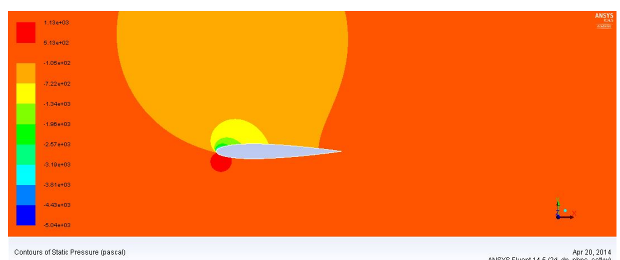

(b) Contours of static pressure at 9° angle of attack with the $k-\omega$ turbulence model

Figure 7: Comparing the contour pressure data obtained from the $k-\omega$ turbulent CFD simulation for the NACA 0012 airfoil.

A. Grid Convergence Index for NACA 0012 airfoil

We are using at least two solutions on different meshes. The GCI is a measure of the percentage on the computed value away from the asymptotic value.[16] The r value is define as $r = \frac{h_2}{h_1}$., where h_1 is the fine simulation and h_2 is the coarse simulation. The order of convergence, p, is theoretically $p = 2$. The f values were calculated for the maximum velocity at zero degree angle of attack where $f1 = 50.99494$ (coarse mesh), $f2 = 51.05993$, and $f3 = 51.26616$ (finest mesh).

Relative error:

$$\epsilon = \frac{f1 - f2}{f1} \tag{5}$$

Table 2: CFD Analysis of Velocity over a NACA 0012 Airfoil

Grid	Grid Spacing	(f values), Max Velocity at 0° AOA	Mesh size
1	4	50.99494	420000
2	4	51.05993	1680000
3	1	51.26616	6720000

Determining the Richardson extrapolation with 2 finest grids to estimate solution at $h = 0$:

$$f_{h=0} \approx f_1 + \frac{f_1 - f_2}{r^p - 1} = 50.99494 + \frac{50.99494 - 51.05993}{2^{1.66596} - 1} = 50.965 \tag{6}$$

By using 3 or more simulations:

$$F_{sec} = 1.25 \tag{7}$$

Determining order of convergence p:

$$p = \frac{ln\frac{f_3 - f_2}{f_2 - f_1}}{ln(r)} = \frac{ln\frac{51.26616 - 51.05993}{51.05993 - 50.99494}}{ln(2)} = 1.6660$$

(8)

Finding the grid convergence index:

$$GCI_{21} = F_{sec}\frac{|\epsilon|}{r^p - 1} \tag{9}$$

$$GCI_{12} = 1.25\frac{\frac{50.99494 - 51.05993}{50.99494}}{2^{1.6660} - 1} = 0.073\% \tag{10}$$

$$GCI_{23} = 1.25\frac{\frac{51.05993 - 51.26616}{51.05993}}{2^{1.6660} - 1} = 0.23\% \tag{11}$$

Determining the asymptotic range of convergence

$$\frac{GCI_{i,i+1}}{GCI_{i+1,i+2}} \approx 1 \tag{12}$$

$$\frac{0.00073}{0.0023}2^{1.6660} = 1.0013 \tag{13}$$

Verification is important for building confidence and credibility in the CFD simulations. The verification aids in determining the accuracy in the computational simulations for the NACA 0012 airfoil. Implementing a verification on the NACA 0012 airfoil shows a correct representation of Eleni's model. By conducting the verification tests the Bumblebee MAV wing CFD simulations can then be validated with its experimental data. From there validation can proceed on the MAV bumblebee wing.

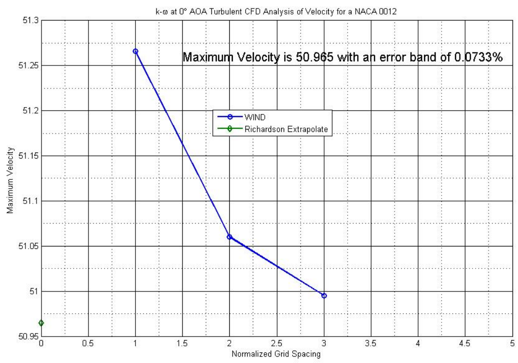

(a) CFD analysis of Maximum Velocity at zero AOA for the NACA 0012 airfoil.

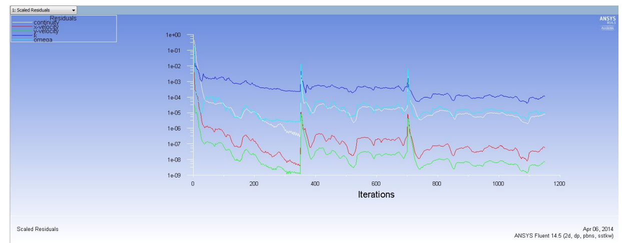

(b) Three different mesh residuals.

Figure 8: Comparing the GCI error analysis and the residuals from the FLUENT solver for the NACA 0012 airfoil.

V. Computational Validation Approach

A finite element wing-box numerical simulation using ANSYS-FLUENT was conducted. This type of wing-box simulation was needed to compute the lift and drag forces on the wing numerically.[3] A transient three-dimensional computational domain for a flapping wing is underway. The gridding is non-uniform. The model is defined by an inlet and an outlet. At the inlet we prescribe a mean velocity of 12.88 m/s as we had in the Wind tunnel experiments. We desire to capture the flow separation near the leading edge. We desire to integrate the pressure field in FLUENT around the wing to yield the total lift and drag. The span is 7 cm, the chord is 3 cm, and the thickness is 0.01 mm. It is surrounded in a computational domain that extends 13 cm in the span wise direction from the wingtip, 21 cm in the chord wise direction from the leading edge and trailing edge and 21 cm above and below the wing.

A. The Steady State Incompressible Navier Stokes Equations

The incompressible steady Navier Stokes equations is given below:

$$-\nu\Delta\mathbf{v} + (\mathbf{v}\cdot\nabla)\mathbf{v} + \nabla p = 0 \tag{14}$$

$$\nabla\cdot\mathbf{v} = 0 \tag{15}$$

By using the appropriate scaling, we have eliminated the density ρ.

This is the vector form of the Navier Stokes equations that we have considered.

The Reynolds number for the bumblebee MAV can be depicted by the equation below: Using this data, we can define a ratio R known as the *Reynolds number* (which can be written in terms of the kinematic viscosity ν_0 if we combine the density and dynamic viscosity μ_0:

$$R \equiv \frac{\rho_0||V_0||L_0}{\mu_0} = \frac{||V_0||L_0}{\nu_0} \tag{16}$$

$$L = \frac{1}{2}\alpha v^2 A C_L \tag{17}$$

The Reynolds number,in one value, shows the scales of length, velocity, mass and viscosity.

To save computational effort, a symmetry plane is put 4 cm from the chord to allow for modeling one wing. A steady-state model is constructed in FLUENT to compare with free stream velocity to determine how many computational cells would be required to accurately capture the lift and thrust (in gram force) to collect the performance of the wings.

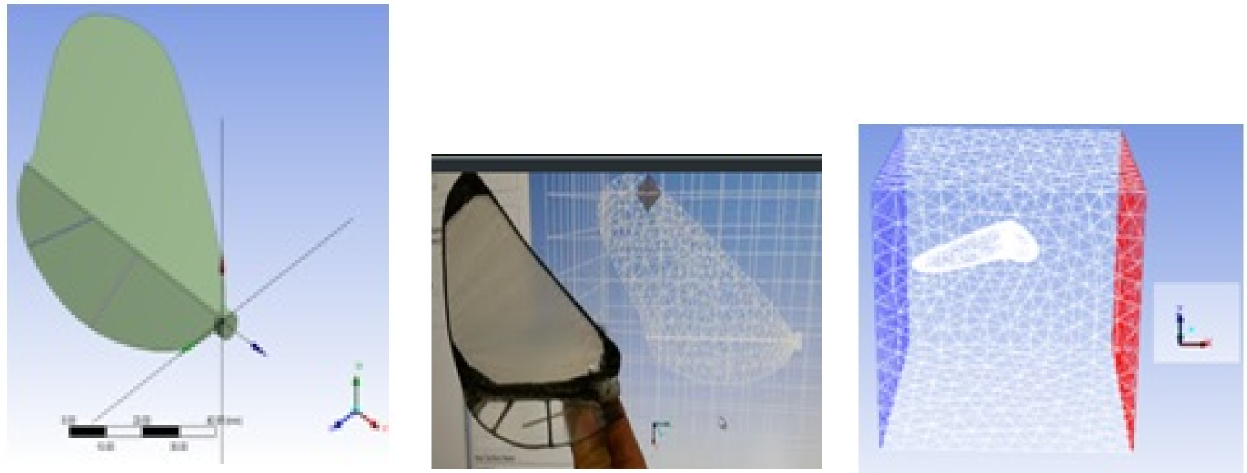

(a) CAD Model of the Bumblebee-wing geometry in ANSYS-Workbench.

(b) Mesh of the CFD-wing with the real-wing.

(c) The fluid domain where the airflow blows from left to right over the computational wing inside a simulated wind tunnel environment.

Figure 9: Comparing the actual wing and the computational wing.

VI. CFD Simulation Results

Steady state simulations for 36 angles of attack have been simulated. 36 Simulations with varying velocity in the x and z components were varied with a magnitude velocity of 12.88 m/s was set at the inlet boundary condition. Converged solutions are reported where the relative residuals drops to less than 10^{-6}.

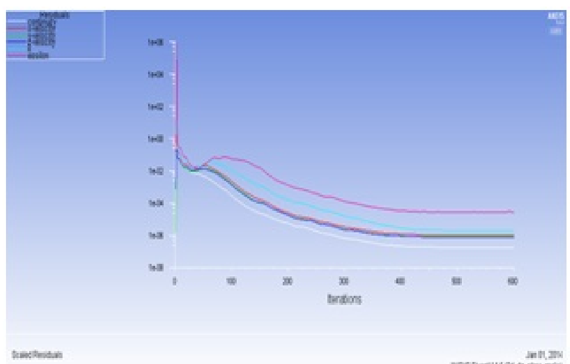

Figure 10: Typical Converging Residuals the simulations Bumblebee MAV-wing experience for running 36 simulations.

The CFD model shows the separation bubbles that surround the trailing edge of the wing. The velocity vectors that surround the bumblebee wing occurs over the rear wing portion rather than the fore wing.

A. Separation Bubbles

The performance of the MAVS is greatly affected by separation bubbles as the MAV flies at low Reynolds number. Separation bubbles are caused by the strong pressure gradient which makes the turbulent boundary layer to separate from the curved surface,[5].[11] The pressure rise is related to the velocity drop towards the trailing edge.

Laminar separation bubbles greatly reduce the L/D ratio. The boundary layer leaves the surface in tangential direction which results in the wedge shaped separation area. Although separated, the laminar flow is sensitive to disturbances, which may lead to the turbulent transition. If the pressure gradient is not

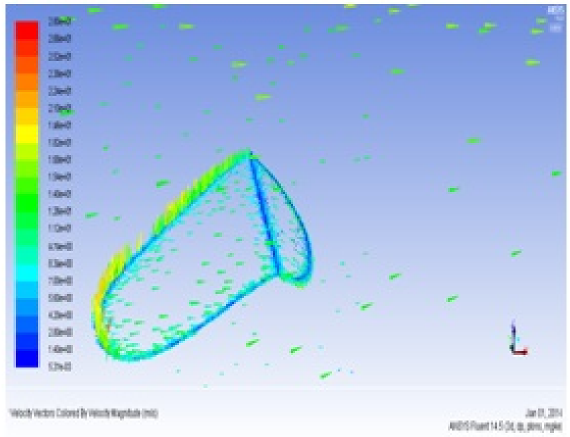

Figure 11: Velocity vectors that display separation of flow up the forewing and down the rearwing.

very strong, the flow can reattach as the turbulent boundary layer. The region where the turbulent flow touches the surface again is called the reattachment point. The volume flow and turbulent flow is called a laminar separation bubble. The flow may be circulating inside the bubble. And there is almost no energy exchange with the outer flow, which makes the laminar separation bubble stable.

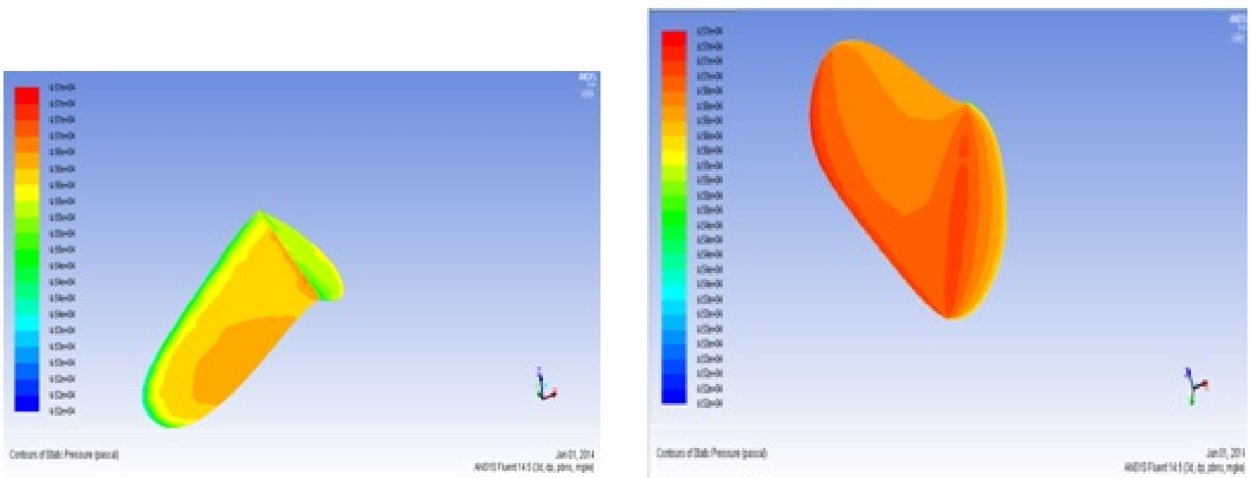

(a) Top Pressure Contours of the CFD wing.

(b) Bottom Pressure Contours of the CFD wing.

Figure 12: Comparing contours of pressure on the top of the wing vs the bottom of the wing at 16° angle of attack.

The contours above shows that a pressure differential gives lift for the bumble wing. The wing experiences high pressure on the bottom and low pressure on the top of the surface of the wing.

Table 3: Grid Refinement Case Study

Mesh	Max Lift Coefficient	Max Drag Coefficient
300k	0.4	0.05
850k	1.6	0.16
Experiment	0.59	0.24

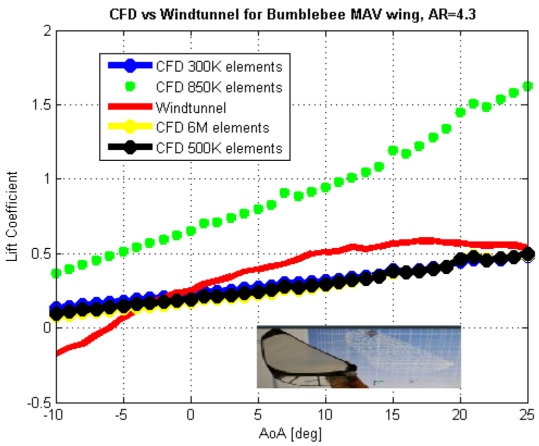

(a) CFD vs Windtunnel Lift Coefficient.

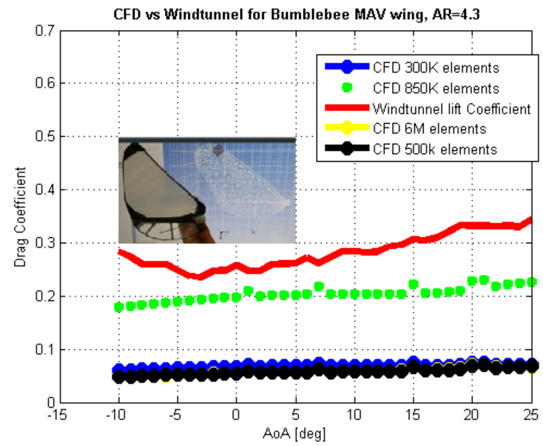

(b) CFD vs Windtunnel Drag Coefficient.

Figure 13: Comparing the lift and drag coefficient vs angle of attack for the CFD model and the real wing.

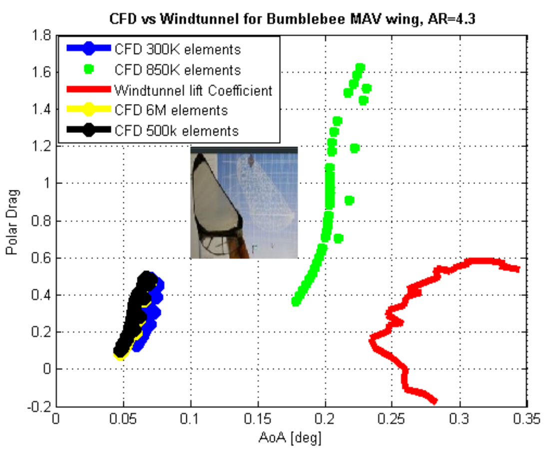

(a) Drag Polar.

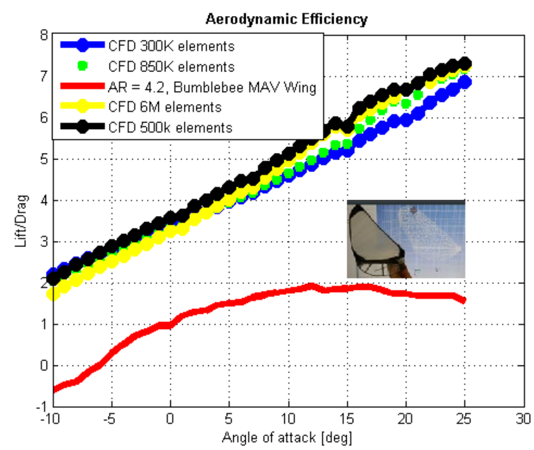

(b) Aerodynamic Efficiency.

Figure 14: Comparing the polar drag and aerodynamic efficiency vs angle of attack for the CFD model and the real wing.

The CFD wing experiences a polar drag at lower angles of attack than the real wing that is postulated to be due to having a low mesh size (300k elements). By comparing the CFD and the real wing one can see that the CFD wing has a greater aerodynamic efficiency than the real wing.

VII. Conclusion

Aerodynamic characteristics are documented for a recently developed bumblebee MAV wing at Arizona State University. Aerodynamic experimental data for the MAV wings were found using the ASU Wind tunnel. It was found that the maximum aerodynamic efficiency for the bumblebee MAV is achieved at approximately 11° angle of attack for Reynolds numbers between 55,000 and 65,000. From the experimental wind tunnel data of the angles of attack from -10° to +25°, it was determined that the stall angle was at 16° AOA. The maximum aerodynamic efficiency is observed to increase with flying speed. A maximum aerodynamic efficiency occurs at $L/D \cong 1.94$ and is observed when flying at 12.88 m/s.

The minimum lift force to reach equilibrium must be 0.0095 N for the bumblebee vehicle to support its own weight. As found through the load cell test, the flapping frequency for the bumblebee is capable of flight. The efficiency is due to how the wing articulates and the rigidity of the wing itself. Load cell tests indicate that lift force in hover exceeds its actual weight. A tradeoff between vectored thrust and torque appears to be negating a portion of the force to maintain hovering stability.

Load cell tests were conducted to determine the flapping frequency and lift efficiency for the bumblebee MAV. The flapping frequency at quarter throttle was around 16 Hz. The test was performed with a tachometer. The no load test of the brushless motor generated a frequency of 122 HZ which is the flapping frequency of a typical bee. The Bumblebee had an average of 2.4 N of force from a load cell test. Wind tunnel experiments determined aerodynamic properties such as the max coefficient of drag, $C_D \cong 0.24$ and coefficient of lift, $C_L \cong 0.59$ for upward moving.

VIII. Acknowledgments

The research in this paper was partially supported by the WAESO-NSF program.

References

[1] R. Dudley and C.P. Ellington. "Mechanics of Forward Flight in Bumblebees I. Kinematics and Morphology" J. exp. Biology. Cambridge University Press, 1990. https://docs.google.com/viewer?a=v&pid=sites&srcid=YXN1LmVkdXxtaWNoYWVsLXRob21wc29ufGd4OmI4MmQyYmNjZDlmNDVlZA

[2] R. Dudley and C.P. Ellington. "Mechanics of Forward Flight in Bumblebees II Quasi-Steady lift and Power Requirements" J. exp. Biology. Cambridge University Press, 1990. https://docs.google.com/viewer?a=v&pid=sites&srcid=YXN1LmVkdXxtaWNoYWVsLXRob21wc29ufGd4OmJkMWM3YzQxYTFlODAxZg.

[3] Manoj K.Bhardwaj, "A CFD CSD Interaction Methodology for Aircraft Wings", Doctorate Dissertation Virginia Polytechnic Institute, 1997. https://docs.google.com/viewer?a=v&pid=sites&srcid=YXN1LmVkdXxtaWNoYWVsLXRob21wc29ufGd4Ojc1NWEwNmRkOWRjYWMzZDA

[4] G. Torres, T. Mueller. Micro Aerial Vehicle Development: Design, Components, Fabrication, and Flight-Testing. University of Notre Dame, 2000. http://www3.nd.edu/~mav/auvsi/torres.htm

[5] D. Gyllhem, K. Mohseni, D. Lawrence. Numerical Simulation of Flow Around the Colorado Micro Aerial Vehicle. University of Colorado. AIAA Fluid Dynamics Conference and Exhibit, Toronto, Canada, june 2005. https://docs.google.com/viewer?a=v&pid=sites&srcid=YXN1LmVkdXxtaWNoYWVsLXRob21wc29ufGd4OjUzNjdkZjFlMmZjNDk3YzQ

[6] Timothy Kinkaides. "Study of Micro -Sized Technology, Micro Air Vehicles and Design of a Payload Carrying Flapping Wing Micro Air Vehicles." Naval Postgraduate School, Monterey, California, March 2006.https://docs.google.com/viewer?a=v&pid=sites&srcid=YXN1LmVkdXxtaWNoYWVsLXRob21wc29ufGd4OjIyNWNmZWE2MjU1MDA1OWM

[7] K. Sarah Shigeoka, "Velocity and Altitude Control of an Ornithopter Micro Aerial Vehicle", University of Utah, Masters Thesis, 2007. https://docs.google.com/viewer?a=v&pid=sites&srcid=YXN1LmVkdXxtaWNoYWVsLXRob21wc29ufGd4OjFmMWM2OWU5OGFkMTE2OGU

[8] G. J. Berman,. and Z. Jane Wang. Energy-minimizing kinematics in hovering insect flight. J. Fluid Mech. vol. 582, pp. 153-168. Cambridge University Press, 2007. https://docs.google.com/viewer?a=v&pid=sites&srcid=YXN1LmVkdXxtaWNoYWVsLXRob21wc29ufGd4OjI5ODlmMTdkMzg1YjljN2E

[9] M. A. Bolender, "Rigid Multi-Body Equations of Motion for Flapping Wing MAVs Using Kanes Equations", U. S. Air Force Research Laboratory, AIAA, 2009. https://docs.google.com/viewer?a=v&pid=sites&srcid=YXN1LmVkdXxtaWNoYWVsLXRob21wc29ufGd4OjdjZmM2OGFhNDdhN2JmMWI

[10] Andrea Serrani, t Benjamin E. Keller, Michael A. Bolender, David B. Doman. "Robust Control of a 3-DOF Flapping Wing Micro Air Vehicle." AIAA Guidance, Navigation, and Control Conference, Toronto, Ontario Canada, August 2010. https://docs.google.com/viewer?a=v&pid=sites&srcid=YXN1LmVkdXxtaWNoYWVsLXRob21wc29ufGd4OjdiZTk1OGI2YWNmMTk2MmI

[11] P. Daniel, "Flapping Wing Design for a Dragonfly-Like Micro Air Vehicle", Masters Thesis, Rochester Institute of Technology, New York, 2011. https://docs.google.com/viewer?a=v&pid=sites&srcid=YXN1LmVkdXxtaWNoYWVsLXRob21wc29ufGd4OjEwYjg2MDcwZDQ2YmVmMDY

[12] Haithem E. Taha, Muhammad R. Hajj, Ali H. Nayfeh. "Flight dynamics and control of flapping-wing MAVs."A review.Springer. Nonlinear Dyn. DOI 10.1007/s11071-012-0529-5, 2012. https://docs.google.com/viewer?a=v&pid=sites&srcid=YXN1LmVkdXxtaWNoYWVsLXRob21wc29ufGd4OjQyZmU0YWEwNjAxODViNWM

[13] Christopher T.Orlowski n, AnouckR.Girard. "Dynamics, stability, and control analyses of flapping wing micro-air vehicles." University of Michigan, Progress in Aerospace Sciences, March 2012. https://docs.google.com/viewer?a=v&pid=sites&srcid=YXN1LmVkdXxtaWNoYWVsLXRob21wc29ufGd4OmZhMzViNmY1NDBkNTcxMQ

[14] J.V. Caetano, J. Verboom, C.C.de Visser. "Near-Hover Flapping Wing MAV Aerodynamic Modelling - a linear model approach." Delft University of Technology, The Netherlands, Portuguese Air Force Research Center, Air Force Academy, Sintra, Portugal, International Micro Air Vehicle Conference and Flight Competition, Toulouse, France, September 2013. https://docs.google.com/viewer?a=v&pid=sites&srcid=YXN1LmVkdXxtaWNoYWVsLXRob21wc29ufGd4OjE2OTllYjFiNjhmODk3ZDg

[15] Eleni C. Douvi, Athanasios T., Dionissios M. "Evaluation of the turbulence models for the simulation of the flow over a National Advisory Committee for Aeronautics (NACA) 0012 airfoil". University of Patras, Greece. Journal of Mechanical Engineering Research Vol 4(3). pp. 100-111, March 2012. DOI: 10.5897/JMER11.074. https://docs.google.com/viewer?a=v&pid=sites&srcid=YXN1LmVkdXxtaWNoYWVsLXRob21wc29ufGd4OjNmYzViOTFhODJkMzM5YWM

[16] Herrmann. M, W.L. Oberkampf. "Verification and Validation in Computational Simulation". Sandia Na-

tional Laboratories, Albuquerque, New Mexico. April 29, 2004.https://docs.google.com/viewer?a=v&pid=sites&srcid=YXN1LmVkdXxtaWNoYWVsLXRob21wc29ufGd4OjdmY2MyYWRlYzBmZjVkYWQ

IX. Bibliography

A. Michael Bibliography

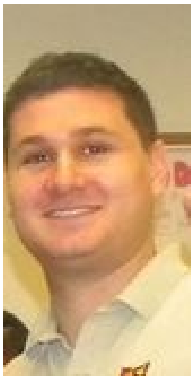

Michael J. Thompson was born in Phoenix, Arizona, on August 6th 1989. He received the B.Sc. degree in Mechanical engineering from Arizona State University in the Ira A Fulton School of engineering in 2012. He will receive his PhD in Mechanical engineering in the field of Modeling, Analysis, Control, Design, and Rapid Prototype of Micro Air Vehicles by 2017.

From December 2010 to 2011 he had participated in five NSF funded Western Alliance to Expand Student Opportunity (WAESO), three NSF funded Fulton Undergraduate Research Initiative (FURI) and one NSF research experience for undergraduates (REU) where he received a patent submission with 2%royalties in a new scientific discovery in drag reduction in computational fluid dynamics research work using ANSYS-FLUENT at the University of Alabama (UA). During the August-October 2011 period, Michael had the opportunity to work at Intel. During the summer of 2013, Michael had an internship with the Ford Motor Company. His job was to use Computational fluid dynamics (CFD) to understand the air flow associated with an automotive vehicle hood creation (metal stamping) tool. The research that he is working on can be found on his personal website: https://sites.google.com/a/asu.edu/michael-thompson/projects/spring-2014. He is the recipient of 2013 GEM fellowship award.

B. Akshay Bibliography

Akshay Batra was born in Delhi, India on Aug 11, 1990. He received the BS in Mechanical and Automation Engineering from Guru Gobind Singh Indrapratha University, Delhi in 2012. In his senior project for the bachelors, he designed an electric vehicle which got him lot of accolades and featured a live radio interview in All India Radio. After completing his bachelors he moved to Arizona State University, United States for his masters in Mechanical Engineering. Since 2013, he has been a research aide in the School of Engineering for Matter Transport and Energy at Arizona State Universitys Thermofluids laboratory. He has been working on thermochemical energy storage. His research interests lies in Energy systems Analysis, fluid mechanics and Computational Fluid Dynamics, which also has been major concentration of his work.

Akshay was a part of the poster conference for Society of Hispanic Professional Engineers for Optimization of the Micro Air vehicles through Bio Mimicry of Bumblebees. In the current work he has mainly been involved in the Computational Fluid Dynamic analysis of the Micro Air Vehicle.

C. Deyzi Bibliography

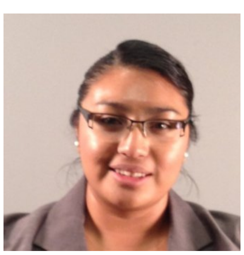

Deyzi Ixtabalan was born in Phoenix, Arizona on January 19, 1990. She received a B.S.E degree in Aerospace engineering from Arizona State University in the Ira A Fulton School of Engineering in 2013. She was a part of the ASU/NASA Space Grant program from November 2011 to December 2013, where she worked with Daedalus Astronautic, ASUs rocketry club and with Science is Fun, an outreach education program. Was a mechanical intern for STARA Technologies during the summer of 2013, were she supported the rapid fielding engineering department. She also participated in three (3)-research project funded by Western Alliance to Expand Student Opportunity (WAESO). Currently pursuing graduate school options.

D. John Bibliography

John S Burnett was born in Spokane Washington, on July 26 1968. He received the B.Sc. degree in Aerospace Engineering from Arizona State University at the Ira A Fulton School of engineering in 2012. Mr. Burnett is currently employed at Honeywell Aerospace, Space and Defense DSES, Glendale, AZ. Mr. Burnett began his engineering career developing pneumatic Mars rover designs in 1994. In 1996 Mr. Burnett successfully developed an autonomous ant like robotic vehicle capable of performing tasks in hostile environments by mimicking behavior of ants.

In early 2004 Mr. Burnett began experimenting with flapping wing aeronautical vehicles, and successfully demonstrated a functional flapping wing design that would be the focus of research at Arizona State University under the supervision of Dr. Armando Rodriguez and Graduate Student Michael Thompson at the Arizona State University School for the Engineering of Matter Transport and Energy, SMTE beginning in the spring of 2012. As an associate researcher on the flapping wing vehicle program, Mr. Burnett with Mr. Thompson have successfully equipped a modern, well funded lab capable of generating successful prototypes as well as computational models, and methods for proof of concept vehicle development .

E. Diana Tran Biblography

Diana Tran was born in Los Angeles, on December 11th 1992. She will be receiving her B.S.E. degree in Mechanical engineering from Arizona State University in the Ira A. Fulton School of Engineering by May of 2014. She plans on pursuing a Masters in Mechanical engineering the following semester. During the summer of 2012, Diana had an internship with Cadence Aerospace, LLC. Her work at Cadence Aerospace included SolidWorks analysis and documentation of current assembly tools, design and development of new tools for part marking and constructing organized work orders for the assembly line employees. Currently she is working in Computational Fluid Dynamics analysis of a bumblebee Micro Air Vehicle wing collecting lift and drag data aerodynamic forces.

X. APPENDIX A

Aerodynamic Calculations

A. 300k Mesh CFD-FLUENT Calculated coefficient of lift and drag data

```
cl_CFD_300kmesh=[0.132234 0.141953 0.151612 0.161047 0.170175 0.179478 0.188535 0.19742 0.206475
0.215529 0.224566 0.239562 0.242166 0.251444 0.260485 0.270145 0.279358 0.303939 0.29763 0.306985
0.316324 0.325958 0.336137 0.345894 0.35526 0.388771 0.376702 0.388081 0.399594 0.411413 0.44636
0.460012 0.450412 0.463626 0.472749 0.485888]
cd_CFD_300kmesh=[0.0600078 0.0608377 0.0616542 0.0624133 0.0631145 0.0638094 0.0644306 0.0649917
0.0655486 0.0660506 0.0665423 0.069979 0.0673173 0.0677268 0.0679824 0.0683083 0.0684976 0.0730343
0.0688369 0.0689364 0.0689841 0.069085 0.0691812 0.0691623 0.0691374 0.0748517 0.0691573 0.0692872
0.0695102 0.0697465 0.0752368 0.0755829 0.0707932 0.0710271 0.0708322 0.0708676]

cd_CFD_850kmesh=[ 0.178282 0.180883 0.183439 0.185811 0.188087 0.190328 0.192346 0.194116 0.195478
0.197065 0.198309 0.210172 0.200347 0.201064 0.201765 0.202391 0.202855 0.217934 0.203559 0.203734
0.203943 0.203969 0.203787 0.20334 0.203298 0.222392 0.205004 0.205543 0.207046 0.209144 0.228357
0.230683 0.217368 0.221165 0.223976 0.22647 ] ;
cl_CFD_850kmesh=[ 0.363336 0.393997 0.42409 0.45366 0.482884 0.511809 0.540546 0.568779 0.595655
0.624773 0.652957 0.704548 0.710138 0.738532 0.767584 0.79655 0.825571 0.907816 0.885063 0.915271
0.946536 0.97813 1.01061 1.04461 1.0816 1.18862 1.17332 1.22072 1.27713 1.33526 1.44789 1.50884
1.48518 1.53423 1.57939 1.62217 ] ;
```

B. Wind Tunnel Raw data

```
Lift=[-0.15 -0.11 -0.09 -0.04 0 0.06 0.1 0.14 0.17 0.2 0.21 0.25 0.27 0.29 0.32 0.33 0.35 0.36
0.39 0.42 0.43 0.44 0.46 0.45 0.46 0.48 0.49 0.49 0.49 0.48 0.48 0.47 0.47 0.47 0.47 0.45]
Drag=[0.24 0.23 0.22 0.22 0.22 0.21 0.2 0.2 0.21 0.21 0.22 0.21 0.21 0.22 0.22 0.22 0.23 0.22
0.23 0.24 0.24 0.24 0.24 0.25 0.25 0.26 0.26 0.26 0.27 0.28 0.28 0.28 0.28 0.28 0.28 0.29]
Temperature=[301.47 301.26 301.41 301.22 301.16 300.92 300.9 301.18 301.28 301.36 301.44 301.41
301.34 301.27 301.23 301.05 300.87 301.13 301.44 301.53 301.56 301.65 301.8 301.7 301.34 301.1
301.29 301.44 301.55 301.5 301.53 301.47 301.45 301.43 301.35 301.3]
Dynamic_Pressure=[93.98 92.88 93.67 93.92 93.69 93.48 93.2 94.38 94.17 93.76 94.52 94.04 93.91
93.89 93.56 93.09 93.87 92.98 93.04 93.53 93.44 94.09 93.74 94.42 93.28 93.87 94.64 92.9 92.92
92.91 93.22 93.26 93.56 93.39 93.86 93.19]
Ambient_Pressure=[97500 97500 97500 97500 97500 97500 97500 97500 97500 97500 97500 97500 97500
97500 97500 97500 97500 97500 97500 97500 97500 97500 97500 97500 97500 97500 97500 97500 97500
97500 97500 97500 97500 97500 97500 97500]
Angle_of_attack=[-10 -9 -8 -7 -6 -5 -4 -3 -2 -1 0 1 2 3 4 5 6 7 8 9 10 11 12 13 14 15 16 17
18 19 20 21 22 23 24 25]
Re=[62837.74 62513.25 62761.03 62806.46 62771.72 62725.18 62759.3 62964.72 62817.38 62801.61
62888.4 62841.71 62742.18 62776.19 62683.34 62620.93 62793.04 62670.78 62548.05 62591.49 62598.3
62686.75 62650.48 62937.97 62558.93 62811.79 63053.44 62368.69 62434.92 62460.8 62543.61 62594.77
62628.46 62485.63 62750.96 62590.27]
Velocity=[12.92 12.84 12.9 12.9 12.89 12.86 12.86 12.93 12.9 12.91 12.93 12.92 12.89 12.89
12.87 12.85 12.87 12.86 12.86 12.88 12.88 12.9 12.91 12.96 12.86 12.89 12.95 12.82 12.84 12.85
12.87 12.87 12.88 12.85 12.9 12.86]
hold on
```

C. Computation of lift and drag coefficient

```
% Calculate lift coefficient
for i = 1:36
Coeff_lift(i)=Lift(i)/(Dynamic_Pressure(i)*Area)
i+1
end
% Calculate drag coefficient
for i = 1:36
Coeff_drag(i)=Drag(i)/(Dynamic_Pressure(i)*Area)
i+1
end
```